INTERFACE

rsif.royalsocietypublishing.org

Research

Cite this article: Reigada R, Sagués F. 2015 Chloroform alters interleaflet coupling in lipid bilayers: an entropic mechanism. *J. R. Soc. Interface* **12**: 20150197.
http://dx.doi.org/10.1098/rsif.2015.0197

Received: 5 March 2015
Accepted: 11 March 2015

Subject Areas:
biophysics, computational biology

Keywords:
lipid bilayer, interleaflet interaction, chloroform, coarse-grained molecular dynamics, anaesthesia

Author for correspondence:
Ramon Reigada
e-mail: reigada@ub.edu

THE ROYAL SOCIETY
PUBLISHING

Chloroform alters interleaflet coupling in lipid bilayers: an entropic mechanism

Ramon Reigada[1] and Francesc Sagués[2]

[1]Departament de Quimica Fisica and Institut de Quimica Teorica i Computacional (IQTCUB), Universitat de Barcelona, c/Martí i Franquès 1, Pta. 4, 08028 Barcelona, Spain
[2]Departament de Quimica Fisica and Institut de Nanociencia i Nanotecnologia (IN2UB), Universitat de Barcelona, c/Martí i Franquès 1, Pta. 4, 08028 Barcelona, Spain

RR, 0000-0003-2177-7014; FS, 0000-0002-2956-5676

The interaction of the two leaflets of the plasmatic cell membrane is conjectured to play an important role in many cell processes. Experimental and computational studies have investigated the mechanisms that modulate the interaction between the two membrane leaflets. Here, by means of coarse-grained molecular dynamics simulations, we show that the addition of a small and polar compound such as chloroform alters interleaflet coupling by promoting domain registration. This is interpreted in terms of an entropic gain that would favour frequent chloroform commuting between the two leaflets. The implication of this effect is discussed in relation to the general anaesthetic action.

1. Introduction

The organization of lipid components of the plasma membrane is crucial in many cellular processes. Segregation of liquid ordered (*lo*) domains from a liquid-disordered (*ld*) phase is responsible of protein lateral aggregation observed in signalling events [1–4]. The latter phenomenon has usually been characterized by the concept of lipid raft [2–4], and although its very existence as stable membrane platforms has been questioned [5], the lateral heterogeneity of lipids and proteins in the plasma membrane and its biological relevance are undisputed. Equally as important as the organization in the bilayer plane is to examine how membrane components are distributed in both leaflets and how these two leaflets are coupled and interact each other [6–9]. Among other examples, interleaflet coupling provides us a mechanism of communication between extracellular receptors and cytoplasmatic agents in many signalling pathways [10], immunological responses that require the alignment of specific lipid phases [9] and cellular sensing processes involving transient receptor potential (TRP) protein channels [11]. Variations of the interleaflet coupling are also responsible for changes in the mechanical state of the membrane and/or its curvature properties, that, in turn, modify, for example, the activity of alamethicin ion channels [12], the enzymatic action of phospholipase A_2 [13] and the visual excitation function performed by rhodopsin [14].

In the context of general anaesthesia, alterations of the transversal membrane distribution of lateral pressures and/or local electrical charges were suggested to play a role in the anaesthetic action [15]. More recently, it has been shown that the K^+ ionic channel involved in nerve transmission contains a lipid sensor helix in the inner leaflet, which determines its gating behaviour [16], and this mode of action is likely to be shared by other types of membrane proteins. Moreover, the connection between the action of general anaesthetics and alterations of the curvature of the cell membrane has been experimentally established [17]. Despite all this evidence, the lack of sistematic studies linking the action of general anaesthetics with the membrane interleaflet behaviour is surprising.

The effect of chloroform ($CHCl_3$, hereafter referred to as chlf) on lipid bilayers has been computationally studied by means of atomistic molecular dynamics (MD) simulations that have revealed important aspects at the molecular detail. First, chlf partitions into different sections of the bilayer, showing a preference to be placed in the two lipid/water interfacial inner regions (*below*

the phosphate lipid groups) [18]. Second, and as a consequence of this behaviour, chlf dramatically alters membrane transversal properties such as the lateral pressure and electrostatic profiles [18,19]. Third, chlf displays a preference to occupy the more disordered regions of the membrane surface, so that in the case of *lo*/*ld* coexistence, chlf molecules are confined to the *ld* phase [19]. One additional feature that will be important on what follows is related to the transversal dynamics of chlf. Chlf molecules display a very dynamic behaviour in the transversal direction and jump from one leaflet to the other at the nanosecond scale [19].

Atomistic MD simulations are extremely useful to extract information at the molecular level, but they are limited to short time (≈200 ns) and length scales (≈10 nm). Instead, coarse-grained (CG) MD cover much longer scales up to those needed to capture, for example, *lo*/*ld* phase segregation in membranes and interleaflet coupling processes. In this paper, a collection of CG–MD simulations of compositionally symmetric bilayers is presented to study the effect of chlf interleaflet coupling, namely how the presence of this compound alters the phase cross-talk between the two leaflets of the bilayer. Our results show a clear alteration of interleaflet coupling by promoting domain registration (alignment of similar lipid phases at both sides of the bilayer) upon addition of chlf. The analysis of the transversal behaviour of chlf and the comparison with other compounds with different polar affinity (carbon tetrachloride and ethanol) unveil the entropic origin of the reported effect.

2. Methods

2.1. Simulation details

CG–MD simulations were carried out for three different types of phosphatidylcholine (PC) membrane systems, generically referred as DUPC/*x*/chol bilayers. Each membrane initially consisted of a random mixture of an unsaturated lipid (DUPC, a PC with two double-unsaturated 16 : 2 oleoyl tails), a saturated lipid (*x*) and cholesterol (chol). Three saturated lipids with different tail lengths have been considered: DLPC (12 : 0, two saturated lauroyl tails), DPPC (16 : 0, two saturated palmitoyl tails) or DSPC (18 : 0, two saturated stearoyl tails). Bilayers were composed of 828 DUPC molecules (42.6 mol%), 540 saturated PC lipids (27.8 mol%) and 576 chol molecules (29.6 mol%), equally distributed in the two leaflets. To ensure correct membrane hydration, 12 600 water beads were used. Two simulations were run for each DUPC/*x*/chol bilayer system: in the absence of chlf and in the presence of 1500 chlf molecules (0.77 chlf molecules per lipid, below the saturation condition of 3–4 molecules per lipid [20]). For the DUPC/DSPC/chol membrane system, additional simulations with 0.26 and 0.51 chlf molecules per lipid were performed as well as with 0.26, 0.51 and 0.77 carbon tetrachloride (CCl_4, hereafter referred to as ctcl) molecules per lipid and 0.77 ethanol (C_2H_6O, hereafter referred as eol) molecules per lipid. In all cases, the non-lipid molecules were added to the membrane system in the aqueous phase and became almost totally (chlf and ctcl) or partially (eol) absorbed by the bilayer after a few nanoseconds.

The simulations were performed using the Gromacs v. 4.5.5 software package [21]. The Martini v. 2.0 force field provided the CG description of the simulated molecules by lumping together an average of four atom groups on a single interaction bead, except for chol, whose ring-like structure is mapped with a higher three-to-one resolution [22]. By the use of Martini force field Risselada & Marrink [23] captured, for the first time, to the best our knowledge, at a molecular detail, the spontaneous segregation of *lo*/*ld* phases in ternary lipid membranes. Since then, this model has been successfully applied to study membrane domain formation and phase behaviour (see [24] and references therein).

The simulations were carried out in the NpT ensemble through a weak coupling algorithm at $T = 295$ K and an anisotropic $p = 1$ atm. Electrostatic interactions were handled using a shifted Coulombic potential energy form, and charges were screened with a relative dielectric constant $\varepsilon_r = 15$. Periodic boundary conditions were used in all three directions, and the time step was set to 20 fs. Owing to the 'smoothing' inherent to the CG potentials, the effective timescale is larger than the actual simulation time. Here, we used the standard conversion factor of 4 [22], which is the speed-up factor needed to obtain the correct diffusional dynamics of CG water particles compared with real water molecules. All membranes were simulated for a period of 12 µs, had an approximate surface of 500 nm^2 (typical linear size about 22.5 nm) and displayed a fluid behaviour. *Lo*/*ld* phase separation and interleaflet coupling processes take place in the proposed simulation time and length scales.

2.2. Voronoi tessellation

Structural analysis of multicomponent DUPC/*x*/chol membranes was performed by the use of Voronoi tessellation. For a given leaflet, phosphate beads of PC molecules and hydroxyl groups of chol molecules were projected onto a plane. The Voronoi tessellation was performed for each leaflet according to the mentioned projections. Because each Voronoi polygon is associated with an individual molecule, membrane properties can be computed, and differential values can be assigned to each component of the membrane.

2.3. Quantification of phase segregation and interleaflet coupling

In order to quantitatively track the *lo*/*ld* segregation process, a segregation parameter was defined. According to the Voronoi tessellation, the lateral (in the same leaflet) neighbours of a lipid molecule can be identified. For a given pair of neighbouring lipids *i* and *j*, the variable $\phi_{i,j}$ is set to +1 if *i* and *j* lipid molecules correspond to the same liquid phase, and equal to −1 otherwise. DUPC molecules were considered to form the *ld* phase, whereas the saturated PC species corresponded to the *lo* phase. Chol molecules were considered to be part of the *lo* phase except in the cases where they had more DUPC neighbours than saturated and other chol molecules. The global segregation parameter can be then defined as $\Phi = <\phi_i>$, where the average was performed for all pairs of lateral neighbour lipids. Strong segregation is then characterized by values of Φ closer to 1.

Similarly, an interleaflet coupling (transversal alignment of phase domains) parameter can be computed. In this case, each lipid molecule had a unique transmembrane neighbour, so the local interleaflet coupling parameter was evaluated by λ_i following the same criteria explained above for lateral neighbours. The global interleaflet coupling parameter was then defined as $\Lambda = <\lambda_i>$, where the average was performed for all lipid molecules *i*. Negative values of Λ correspond to antiregistration of segregating phases, whereas positive values of Λ stand for registration (phase alignment) of lipid domains.

2.4. Simulations of smaller and simpler bilayer systems

In order to check the simulation and equilibration protocols, additional simulations of smaller and simpler bilayers were performed. These bilayers corresponded to the three different types of transversal membrane patches: a symmetric disordered (*ld*–*ld*) bilayer made of 200 DUPC molecules, a symmetric ordered (*lo*–*lo*) bilayer made of 144 DPPC and 144 chol molecules, and

a asymmetric (*lo*–*ld*) bilayer made of a layer with 72 DPPC and 72 chol molecules, and a layer with 64 DUPC molecules. The three small bilayer systems were hydrated with 2000 water beads and equilibrated until the total area converged. The typical linear size of the equilibrated small membranes was approximately 8.4 nm. Simulations were then performed upon addition of 200 chlf molecules (about three chlf molecules per nm^2 of membrane as in the large DUPC/x/chol systems) for a period of 3.2 µs under different conditions. We focused on the transversal probability distribution of chlf molecules in order to check and validate the proposed simulation conditions.

Three different checks were performed with these small membranes. First, a drastic reduction of chlf molecules (up to eight times) did not lead to significant changes in their transversal distribution, showing that the partition of chlf molecules into the bilayer is not governed by direct chlf–chlf interactions at the fractions used in our simulations. Second, we checked the use of different coupling schemes for temperature and pressure, and we found that chlf behaviour is not significantly altered by the use of Nosé–Hoover thermostat and Parrinello–Rahman barostat instead of Berendsen weak coupling approaches. Third, the use of polarizable water [25] did not modify the transversal chlf behaviour either.

Finally, umbrella sampling [26] was used to calculate the free energy profiles (potential of mean force, PMF) for a chlf molecule traversing the asymmetric *lo*–*ld* bilayer. First, additional water slabs were added (up to a total of 6000 water beads), and the system was equilibrated again. By adding extra water particles, the size of the system was almost duplicated in the z-direction, so we could sample the whole membrane thickness plus a large portion of the aqueous phase and avoid, at the same time, possible artefacts owing to periodic boundary conditions. PMF(z) was then calculated for a length of 8 nm traversing the membrane in a series of 80 independent simulation windows with the centre of mass of chlf fixed by a harmonic constraint around z positions in 0.1 nm steps. Each umbrella simulation window was performed for 100 ns (20 ns of equilibration). The analysis of the umbrella simulations was performed using the weighted histogram analysis method [27].

At this point, it is worth noting that special care has to be taken with free energy estimations from a CG force field. The Martini description for chlf neither possesses any distribution of charges nor accounts for its polarizability, and these simplifications are especially important when working with media of different polarities. Because the CG approach 'softens' the energy landscape, the energy barriers are reduced leading to an underestimation of the chlf partitioning to the membrane [28]. Despite this discrepancy, the chlf PMF computed from Martini simulations reproduced the general shape obtained from all-atom and captures the key interactions responsible for partitioning into the membrane [28]. This agreement is relevant for us, because the discrepancy with the water/membrane partition is not as important for our results than the fact that the chlf molecules partition inside the membrane is rather similar to that obtained from atomistic approaches.

2.5. Simulations to check the effect of system size and ionic strength

The analysis of interleaflet coupling has been performed in membranes made of 1944 lipid molecules corresponding to membrane surfaces of the order of 500 nm^2. This membrane size is standard in many of the most recent simulations using CG simulations on lipid membranes [24,29–32]. However, when the simulated process leads to the formation of membrane domains that become of the order of the system's size possible finite size effects have to be checked. We thus conducted two additional simulations for a 2×2 replica of the initially mixed DUPC/DSPC/chol membrane system. The enlarged membrane contained 7776 lipid molecules and 50 400 water particles, summing up a total of 138 816 beads, and its lateral size was of the order of 45 nm (a surface of about 2000 nm^2). This membrane was simulated both in the absence of chlf and in the presence of 6000 chlf molecules (the same ratio of 0.77 chlf per lipid used in the original membrane) up to 4.8 µs. Visual inspection of the evolution of the enlarged membranes revealed a consistent effect of chlf on the transversal behaviour of segregating domains, and the computation of the interleaflet coupling parameter Λ for the simulated period did not lead to any significant modification with respect to the results for the standard membranes reported in the following sections. Finite size effects on the transversal behaviour reported in this paper can be therefore discarded.

Because biomembranes are generally immersed in an aqueous medium with high ionic strength, we also checked the effect of electrolytes in our results. We simulated the DUPC/DSPC/chol membrane system (with and without chlf) in the presence of Na^+ and Cl^- 0.15 M (similar to the typical physiological ionic strength). The effect of chlf on transversal domain synchronization was fully reproduced in these simulations in accordance with the results in the absence of electrolytes.

3. Results

3.1. The simulated membranes display *lo*/*ld* phase segregation

Temporal evolution of the three large DUPC/x/chol membrane systems displays phase separation: the saturated lipid (x = DLPC, DPPC or DSPC) forms a packed lipid phase (*lo*) together with chol molecules, segregated from a disordered phase rich in DUPC (*ld*). A sequence of the segregation process is shown in figure 1 for one of the layers of the DUPC/DPPC/chol membrane system. The temporal evolution of the segregation parameter Φ is also plotted for the three simulated systems.

Addition of chlf has a minor influence on the kinetics and the *extent* of the phase separation process (figure 1). This observation does not imply that chlf has no effect on the lipid mixture phase stability. It is likely that addition of this compound to a lipid membrane may alter its phase behaviour when placed close to a phase boundary or to critical conditions. Actually, recent experiments [33] showed that anaesthetics like chlf have a strong influence on plasma membranes close to a phase boundary, lowering its critical temperature. The study of this scenario by means of CG molecular simulations is therefore appealing but beyond the scope of this paper. Here, the mixture was placed well inside the *lo*/*ld* coexistence region, so phase segregation could be observed on an accessible timescale, and a clear analysis of domain behaviour could be performed.

3.2. Realistic lateral diffusion rates are obtained

To open the scope of our simulations and better validate them, lateral diffusivities of the membrane components were calculated. Lateral diffusion rates of DUPC computed from our simulations are of the order of $8–9 \times 10^{-8}$ $cm^2\ s^{-1}$ (table 1) and correspond to typical phospholipid mobilities in an *ld* phase [34,35]. Saturated PC lipids forming the *lo* phase display a mobility reduced by a factor of 2 ($4–5 \times 10^{-8}$ $cm^2\ s^{-1}$). These values are in agreement with the experimental observations, which report relative diffusivity ratios

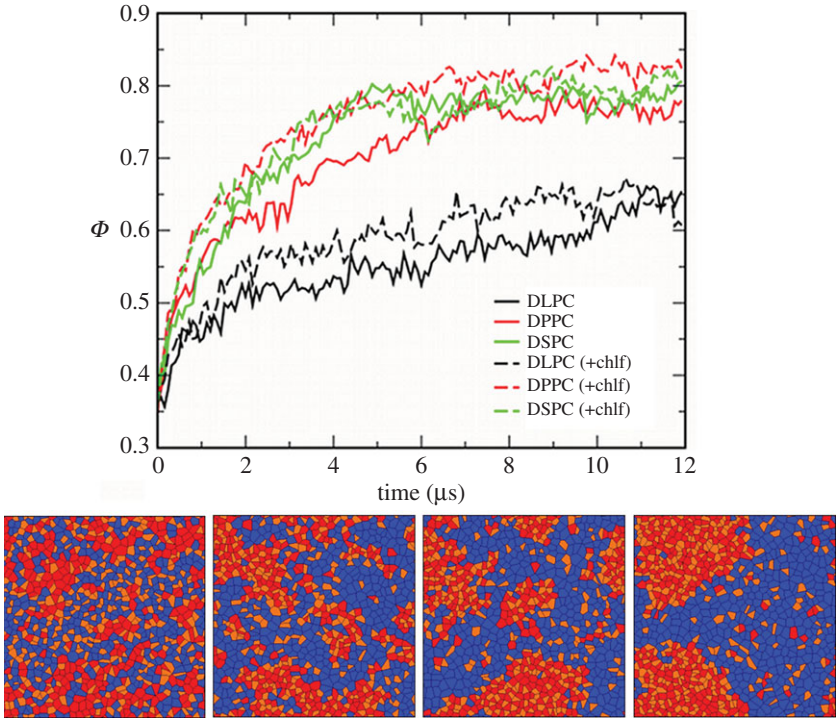

Figure 1. (Top) Temporal evolution of the segregation parameter Φ. DUPC/*x*/chol membranes where $x =$ DLPC (black), DPPC (red), DSPC (green). Solid lines correspond to chlf-free systems, whereas dashed lines stand for bilayers with 0.77 chlf per lipid. (Bottom) Sequence of the phase segregation process observed in one of the leaflets of the simulated DUPC/DPPC/chol membrane system in the absence of chlf. Voronoi polygons are filled with a colour that identifies each one of the lipid components: DUPC (blue), DPPC (red) and chol (orange). DPPC and chol segregates in a more packed phase (*lo*) than the one formed by DUPC (*ld*). From left to right, $t = 0$, 0.4, 1.6 and 12 μs.

Table 1. Lateral lipid diffusivities (rows) for the three DUPC/*x*/chol simulated membranes (columns)[a,b].

	$x =$ DLPC	$x =$ DPPC	$x =$ DSPC
DUPC	8.8 ± 0.4	8.9 ± 0.2	8.1 ± 0.4
	14.5 ± 0.3	*11.1 ± 0.3*	*11.3 ± 0.3*
x	5.1 ± 0.4	4.2 ± 0.3	4.3 ± 0.4
	6.5 ± 0.5	*4.5 ± 0.2*	*4.9 ± 0.3*
chol	7.7 ± 0.4	7.7 ± 0.5	7.9 ± 0.4
	12.4 ± 0.6	*9.40 ± 0.4*	*11.9 ± 0.5*

[a]Diffusion constants were computed from the linear fitting of the mean squared displacement in the 8–12 μs period and they are provided in 10^{-8} cm^2 s^{-1}.

[b]Values in italics correspond to the systems with 0.77 chlf per lipid.

of 2–10 depending on membrane composition [34–37]. Chol molecules display a diffusivity of the order of $7–8 \times 10^{-8}$ cm^2 s^{-1}. Lateral diffusivities provided here are also in agreement with the mobilities obtained in other CG [8,23] and atomistic [38] MD simulations. According to our simulations (table 1), addition of chlf slightly increases lipid lateral mobilities as it could be expected owing to its disordering effect on lipid membranes [18].

Our results also contribute to the recent interest in the influence of the dual-leaflet structure of the membrane on lateral diffusivities. The dual-leaflet continuum model proposed by Wang & Hill [39] leads to high lateral diffusion constants of the order of several μm^2 s^{-1}, much larger than the obtained from the widely adopted Saffman–Delbrük theory. The diffusivities computed from our MD simulations are also of the order of several μm^{2}s^{-1}, thus favouring the dual-leaflet model and, consequently, the membrane leaflet viscosities inferred from this approach [39].

3.3. Length of saturated lipids determines interleaflet phase symmetry

The final snapshots for the two leaflets of the three DUPC/*x*/chol membranes are shown in figure 2 (left panels) in the absence of chlf. Already from visual inspection, the present results agree with those reported in [8]. The membrane containing the longest-tail lipid (DSPC) shows a clear antiregistration behaviour (*lo* and *ld* are not aligned in the two leaflets). Instead, membranes containing DPPC or DLPC present an alignment of the segregating domains (registration). The thickness of a piece of membrane with the two leaflets in an *lo* phase made of DSPC and chol molecules is much larger that the *ld* phase composed by DUPC lipids. According to the simulations, membrane thicknesses (distance between phosphate groups at opposite leaflets) of transversal DUPC–DUPC and DSPC–DSPC pairs are approximately 3.8 and 4.7 nm, respectively. Such thickness mismatch plays against transmembrane colocalization of equal phases and promotes phase asymmetry (DUPC/DSPC/chol system in the left panels of figure 2). Thickness of DPPC–DPPC and DLPC–DLPC transversal pairs leads to 4.2 and 3.8 nm, respectively, much closer to the thickness of a DUPC *ld* membrane patch, so phase alignment is favoured in these two cases.

The interleaflet coupling parameter Λ has been tracked with time and plotted in the central panel of figure 2 for the simulated systems. Clearly, the DUPC/DSPC/chol bilayer displays antiregistration (negative values of Λ), whereas the membranes composed by DPPC or DLPC show positive values for Λ (phase registration).

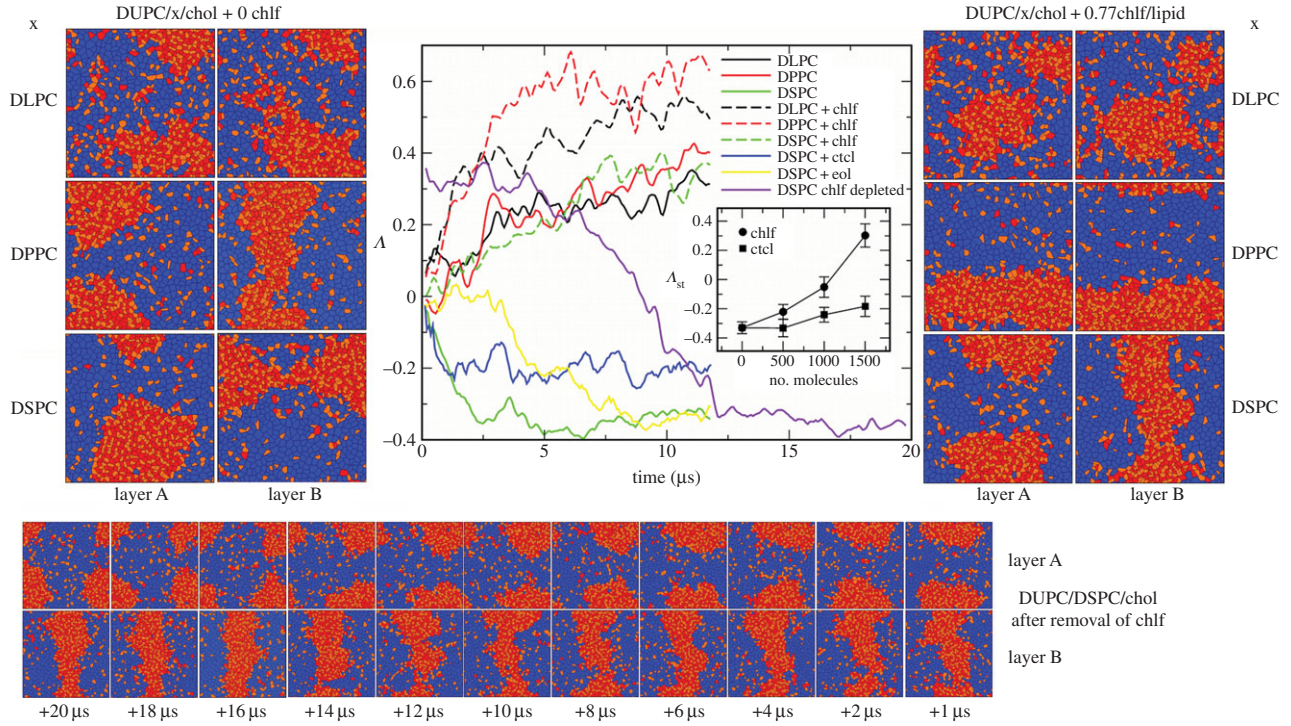

Figure 2. (Left) Final snapshots of each leaflet of the simulated DUPC/*x*/chol membrane systems in the absence of chlf. First row, $x =$ DLPC. Second row, $x =$ DPPC. Third row, $x =$ DSPC. Voronoi polygons are filled with a colour that identifies each of the lipid components: DUPC (blue), saturated lipid $\times$ (red) and chol (orange). (Centre) Temporal evolution of the interleaflet coupling parameter Λ. DUPC/*x*/chol membranes where $x =$ DLPC (black), DPPC (red), DSPC (green). Solid lines correspond to chlf-free systems and dashed lines stand for bilayers with 0.77 chlf per lipid. Blue and yellow correspond to the DUPC/DPSC/chol bilayer with 0.77 ctcl and 0.77 eol molecules per lipid, respectively. The violet line stands for the evolution of the final configuration of the DUPC/DSPC/chol + 0.77chlf per lipid system once the chlf molecules were removed. Inset: stationary value for the coupling parameter Λ_{st} (averaged over the last 4 μs) at different chlf and ctcl contents for the DUPC/DSPC/chol system. (Right) Final snapshots of each leaflet of the simulated DUPC/*x*/chol membrane systems in the presence of 0.77 chlf molecules per lipid. (Bottom) Temporal evolution (from right to left) of each leaflet of the final DUPC/DSPC/chol + 0.77chlf/lipid membrane system once chlf molecules are removed (violet line in the central panel).

3.4. Chloroform favours transversal phase registration in the membrane

Visual inspection of the final snapshots for the three chlf-containing bilayer systems plotted in the right panels of figure 2 reveals the powerful influence of chlf in promoting phase synchronization. In agreement, the coupling parameter Λ increases in each of the simulated membranes when chlf is added to the system (central panel of figure 2). The effect is quantitatively significant for the cases with DPPC and DLPC, and dramatic for the DUPC/DSPC/chol membrane. In this latter case, addition of chlf converts complete domain antiregistration into a more symmetric transversal configuration. As shown in the inset of the central panel of figure 2, the effect is roughly proportional to chlf content.

It is important to note that the reported effect is robust and independent of the initial bilayer configuration. For example, the bottom panel sequence of figure 2 shows that removal of chlf to the final DUPC/DSPC/chol + 0.77chlf/lipid phase-aligned membrane system results in transversal antiregistration in approximately 10 μs (violet line in the central panel of figure 2).

3.5. Chloroform enhances cholesterol flip–flop

As a consequence of promoting registration, chlf has also important effects on the transport of chol across the membrane. The analysis of transmembrane transport was performed by tracking the orientation of individual lipid molecules every 200 ps during a simulation period of 1 μs. No phospholipid flip–flop occurred in any of the simulated membranes, in agreement with the slow phospholipid passive translocation measured experimentally (from hours to days [40]). Instead, recent experimental evidence suggested that chol flip–flop takes place on the submicrosecond timescale [41]. Visual inspection of the orientation of chol molecules revealed a clear dependence on the surrounding phasic state (not shown): chol molecules residing in the *lo* phase remained rather perpendicular to the membrane plane, whereas when residing in the *ld* phase, they were able to enter the bilayer interior adopting a horizontal position and, either return back to the same leaflet or change the leaflet (flip–flop). According to our simulations, chol translocation events take place on the submicrosecond timescale with rates of 0.97–2.25 μs^{-1} (see table 2 for the DUPC/DPPC/Chol and DUPC/DSPC/Chol membranes) showing good agreement with other molecular CG simulations [23,42,43].

In table 2, the distribution of chol flip–flop events with respect to the phasic state of donor and acceptor lipid phases is also provided. Most of the translocation events take place between *ld* transversally coincident domains, only a few of them involve domains at different phasic state, and chol flip–flop rarely occurs between *lo* phases. Accordingly, the lowest rate was obtained for the DUPC/DSPC/chol, whereas changing DSPC by DPPC as a saturated lipid favours transbilayer domain registration, increasing the flip–flop rate. Importantly, addition of chlf in both cases strongly enhances transmembrane chol transport, because

Table 2. Chol flip–flop rates for two simulated systems (columns) without and with chlf (rows). Flip–flop distribution with respect to the phasic nature of donor and acceptor lipid phases[a,b].

	DUPC/DPPC/Chol		DUPC/DSPC/Chol	
no chlf	1.41 μs^{-1}	87.7% *ld*–*ld*	0.97 μs^{-1}	67% *ld*–*ld*
		12.3% *lo*–*ld*		33% *lo*–*ld*
		0% *lo*–*lo*		0% *lo*–*lo*
0.77 chlf per lipid	2.25 μs^{-1}	90.5% *ld*–*ld*	2.01 μs^{-1}	78.8% *ld*–*ld*
		9.1% *lo*–*ld*		18.5% *lo*–*ld*
		0.4% *lo*–*lo*		2.7% *lo*–*lo*

[a]Flip–flop rates were computed by tracking the orientation of chol molecules every 200 ps during 1 μs of simulation.
[b]The phasic nature of the donor and acceptor lipid phases was assigned following the same criteria to compute the segregation and interleaflet coupling parameters Φ and Λ.

chlf favours transversal coincidence of *ld* lipid domains. Modification of chol translocation rates may affect the mechanical response to changes in membrane shape [44], as well as many cellular functions where chol asymmetric distribution is important.

3.6. Chloroform favours the flat conformation

Another important aspect is related to the suppression of local curvature regions upon addition of chlf. Transversal coincidence of *lo* and *ld* domains leads to high local curvatures, whereas the transversal coexistence of equal lipid phases promotes a planar conformation of the membrane. The latter is therefore favoured by chlf. A clear and illustrative example of this effect is shown in figure 3 for a cross-sectional view of the simulated DUPC/DSPC/chol membrane.

As reported above, many signalling [11,14], enzymatic [13] and nerve transmission [12,17] events are modulated by changes in membrane curvature and/or the resultant modifications of internal mechanical stresses and elasticity. In a heterogeneous membrane, bending rigidity can be only defined unambiguously for each segregated single phase, and generally, *lo* phases are rather rigid ($\kappa_{lo} > 60\, k_BT$), whereas disordered *ld* phases are more flexible ($\kappa_{ld} = 0$–$30\, k_BT$) [45]. According to the single-bilayer bending mechanism (dominant for thermal shape fluctuations), the membrane bending modulus can be estimated as the sum of the stiffness parameters of each leaflet [46]. Transversal coincidence of the two lipid phases in the membrane leads to spatial distribution of membrane stiffness: rigid ($\kappa_{lo} + \kappa_{lo}$) pieces of membrane corresponding to coincident *lo*–*lo* domains, and flexible ($\kappa_{ld} + \kappa_{ld}$) pieces corresponding to *ld*–*ld* coincidence. Transversal antiregistration, instead, leads to a different situation: a large portion of the membrane is formed by asymmetric *lo*–*ld* regions whose bending modulus has an intermediate value ($\kappa_{ld} + \kappa_{ld} < \kappa_{lo} + \kappa_{ld} < \kappa_{lo} + \kappa_{lo}$).

3.7. Chloroform and phase registration: an entropic mechanism

Inspection of chlf distribution in the membrane provides the clues to explain the observations reported above. First, the lateral distribution of chlf molecules clearly shows that they preferentially occupy the more disordered (*ld*) regions of the membrane (figure 4). The fraction of chlf molecules that are proximal to the DUPC lipids is approximately 70–80%

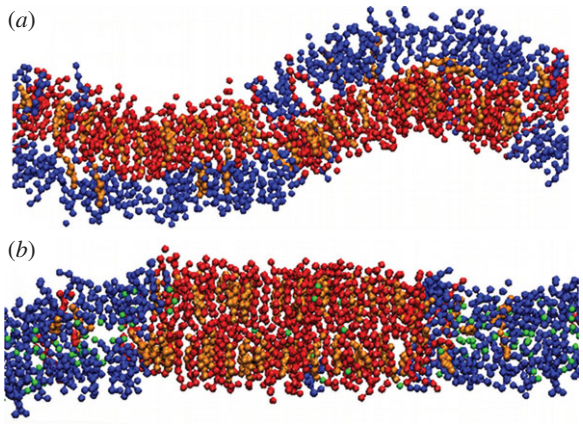

Figure 3. (*a*) Snapshot in the (*x*, *z*) view for a DUPC/DSPC/chol membrane slice. Beads of different colours are used for DUPC (blue), DSPC (red) and chol (orange). Water molecules are not plotted. (*b*) Addition of 0.77 chlf molecules per lipid (green beads) promotes phase symmetry (registration) and as a consequence a planar membrane conformation is favoured.

depending on the simulated membrane and implies an increment of chlf population of 65–86% with respect to a random distribution (table 3). Instead, species forming the *lo* phase show a clear depletion of chlf with respect to a random distribution. The preference of chlf to laterally reside in *ld* phases and avoid *lo* regions was already observed in atomistic MD simulations [19].

Second, each membrane has been analysed in its three different transversal regions: *ld*–*ld* and *lo*–*lo* regions are defined as those patches of the membrane where the segregating phases (*ld* and *lo*, respectively) overlay in the two leaflets (phase registration), whereas mixed transversal patches are referred to as *lo*–*ld* regions, where disordered and ordered lipids are transversal neighbours (phase antiregistration). The corresponding chlf distribution profiles, ρ_z, have been computed and show that chlf molecules occupying *ld*–*ld* regions span the hydrophobic part of the membrane with a particular preference for the inner region of the lipid/water interface of each leaflet (black in figure 5*a*). A typical transversal trajectory of a single chlf molecule residing in an *ld*–*ld* region is plotted in figure 5*b* and shows very dynamic behaviour with jumps from one leaflet to the other taking place at the nanosecond scale [19], much faster than the typical microsecond scales for the flip–flop of chol. The few molecules residing in *lo*–*lo* regions are more confined to the central hydrophobic region with

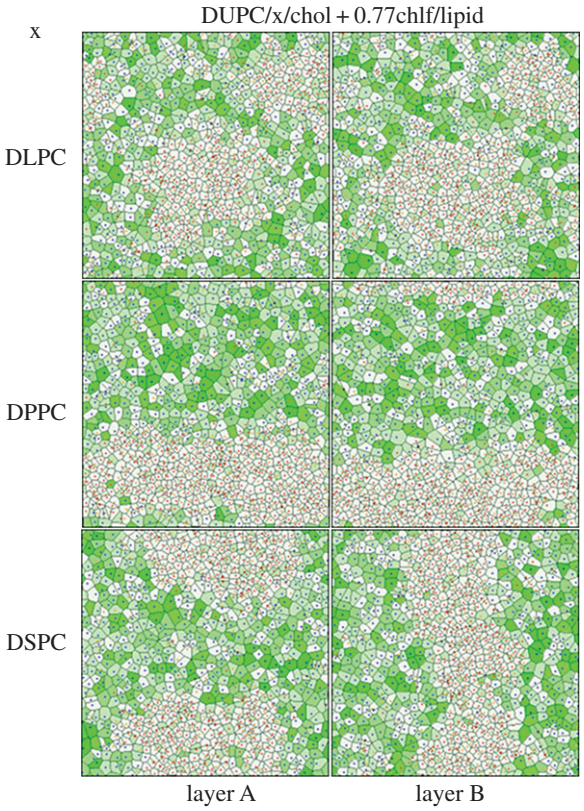

Figure 4. Final snapshots of each leaflet (A/B) of the simulated DUPC/*x*/chol membrane systems in the presence of 0.77 chlf molecules per lipid. First row, $x =$ DLPC. Second row, $x =$ DPPC. Third row, $x =$ DSPC. Voronoi polygons are filled with a green colour scale proportional to the number of chlf molecules close to each lipid molecule. The lipid components are identified by a dot plotted at the centre of the corresponding Voronoi polygon: DUPC (blue), saturated lipid × (red) and chol (orange).

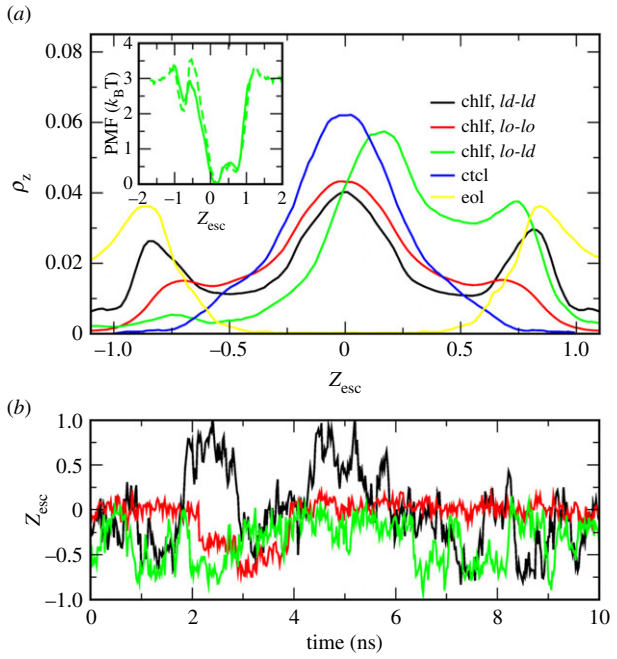

Figure 5. (*a*) Chlf distribution probability in the *z*-axis (normal to membrane surface), ρ_z, for different transversal membrane patches. Profiles are computed from the chlf trajectories in the DUPC/DSPC/chol + 0.77chlf/lipid membrane at $t > 4$ μs (similar behaviour is found for the other two simulated membrane systems) and normalized for each transversal patch: *ld*–*ld* (black), *lo*–*lo* (red) and *lo*–*ld* (green). In blue and yellow, distribution of ctcl and eol molecules, respectively, in the DUPC/DSPC/chol membranes at $t > 4$ μs (in both cases, the distributions for different transversal regions are similar). The profiles are plotted in a scaled distance with respect to the bilayer centre, Z_{esc}, where the position of the opposite phosphate beads are fixed to $Z_{esc} = \pm 1$. The inset shows the PMF profile for chlf computed from the density distributions in *lo*–*ld* membrane regions (solid) and by means of the umbrella sampling method in a small *lo*–*ld* membrane (dashed once rescaled). (*b*) Examples of trajectories of single chlf molecules tracked for a short period of time in *ld*–*ld* (black), *lo*–*lo* (red) and *lo*–*ld* (green) regions. For data corresponding to the asymmetric region (*lo*–*ld*), negative values of the scaled distance correspond to the *lo* leaflet.

Table 3. Location of chlf in the three simulated membranes (columns) with 0.77 chlf molecules per lipid[a].

	$x =$ DLPC	$x =$ DPPC	$x =$ DSPC
DUPC	70.2% (+65%)	79.2% (+86%)	78.0% (+83%)
x	11.2% (−60%)	6.7% (−76%)	7.0% (−75%)
chol	18.6% (−37%)	14.1% (−52%)	15.0% (−49%)

[a]First three rows: percentage of chlf molecules proximal to a given lipid compound. In parentheses, percentage of chlf enrichment/depletion with respect to the average value for a random distribution.

sporadic and short excursions to the interfacial sections (red in figure 5*a*,*b*). The relevant result comes out when examining the behaviour of chlf in the *lo*–*ld* regions. Individual trajectories of chlf molecules in phase-asymmetric regions reveal confinement to the leaflet in the disordered state (green in figure 5*b*). The corresponding chlf distribution profile shows a clear asymmetric distribution (green in figure 5*a*): chlf molecules are mostly found in the disordered leaflet, and only rarely occupy the ordered layer (note that negative values of the scaled distance corresponds to the *lo* leaflet). In agreement, the free energy profile, PMF(z), for a chlf molecule inside an asymmetric *lo*–*ld* membrane patch (inset of figure 5*a*) displays a very low energy barrier to jump to the interfacial region of the disordered layer (0.4 k_BT), whereas the barrier to penetrate the ordered layer is about eight-times higher. The PMF(z) profile has been computed for the chlf molecules residing in the *lo*–*ld* regions of the DUPC/DSPC/chol membrane using the standard expression $\mathrm{PMF}(z) = -k_B T \ln(\rho_z/\rho_0)$, where ρ_0 is the distribution probability at the centre of the bilayer. This expression is valid for molecules that significantly penetrate the membrane, as is the case for chlf. A similar profile is obtained by means of the umbrella sampling method applied to the small *lo*–*ld* asymmetric membrane system (inset of figure 5*a*). The latter observation unveils the mechanism by which chlf promotes phase symmetry. Chlf molecules try to rapidly (nanosecond scale) jump from the lipid/water interfacial section of one leaflet to the other. Because most chlf molecules laterally occupy *ld* regions, the colocalization of these regions at both sides of the bilayer favours such dynamic behaviour, whereas transversal confinement of chlf molecules to one of the leaflets in the *ld*–*lo* regions acts against such randomization and is thus entropically disfavoured (figure 6).

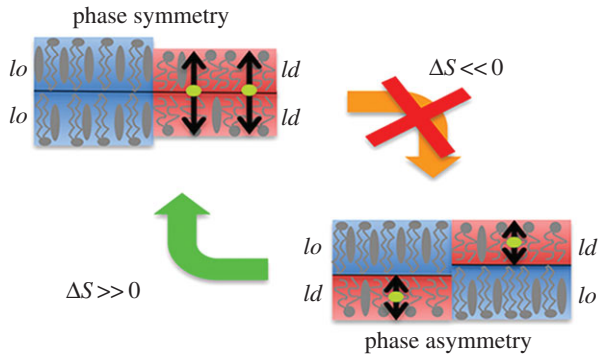

Figure 6. Illustration of the entropic linking mechanism that explains the interleaflet coupling effect of chlf molecules (green) in phase separating lipid bilayers. Double-tailed lipids and chol are shown schematically in grey ordered domains are plotted in red shading and disordered domains in blue shading.

3.8. The cases of carbon tetrachloride and ethanol

The relevant molecular characteristics of chlf that gives rise to its coupling effect is its moderate polar affinity, which causes this compound to partition inside the bilayer with a preference to interact with the lipid/water interface at both leaflets. Simulations with ctcl (considered in the Martini force field as a molecule with null polar affinity) confirm this rationale. As has been previously observed in atomistic simulations [19], ctcl molecules, lacking in polar affinity, are preferentially located at the more inner hydrophobic region of the membrane (blue in figure 5*a*), so they perform trajectories around the bilayer centre that are more confined than those displayed by chlf molecules. Consequently, ctcl only induces a tiny coupling effect as observed in the blue curve in the central panel of figure 2, where the coupling parameter is shown to be increased much less by the presence of ctcl than by chlf.

Compounds with a large polar character, for instance ethanol, are more prone to occupy the lipid/water interfacial regions but avoiding the inner hydrophobic bilayer core [47]. Simulations with ethanol (considered in the Martini force field as a polar bead) in our membrane systems reproduce this behaviour for the eol transversal probability distribution (yellow in figure 5*a*). Interestingly, because eol molecules rarely traverse the hydrophobic section of the membrane, no synchronizing effect is found for this compound in DUPC/DSPC/chol membranes (yellow in the central panel of figure 2).

3.9. Quantification of the entropic effect

Interleaflet coupling is determined by different contributions [6]. In the absence of chlf, phase alignment results from the balance of two interdomain tensions. First, the surface tension, γ_{inter}, promotes phase alignment owing to the unfavourable contact between different lipid phases at the interleaflet surface [48]. The second competing tension corresponds to an intraleaflet line tension, γ_{thick}, caused by the height mismatch between ordered and disordered phases. This tension acts against phase alignment and is increased if the thickness of aligned *lo*–*lo* regions is much larger than *ld*–*ld* regions [8]. The two competing tensions have a different impact depending on the size of the lipid domains: γ_{inter} is a surface tension (energy per surface unit), whereas γ_{thick} is a line tension (energy per length unit). Therefore, as the domain area increases more quickly than its perimeter, larger domains are expected to always be in registration (the surface contribution wins). This explains why domain registration is always observed by optical microscopy. However, if lipid domains develop at smaller (nanometric) scales, intraleaflet line tension may eventually dominate and lead to interleaflet antiregistration, as it is observed in the simulations for the DUPC/DSPC/chol membrane.

Inclusion of chlf adds a third (entropic) contribution. A rough (upper) estimation of this latter effect can be performed by assuming that chlf molecules are much more mobile in the transversal direction than in the membrane plane (lipids are placed in a 'vertical' position, reducing the lateral mobility of chlf) [19]. In the limit of ideal particles moving only in the 'vertical' direction, the variation of entropy owing to the confinement of N chlf particles from a system of length L to $L/2$ corresponds to $\Delta S_{chlf} = \ln(1/2)Nk_B$, namely to a positive contribution to the free energy, $-T\Delta S_{chlf} = -\ln(1/2)Nk_BT$ that promotes phase symmetry. The magnitude of this entropic contribution is found to be relevant with respect to the enthalpic terms discussed above. The interleaflet surface tension, γ_{inter}, has been estimated by a molecular mean-field model (0.01–0.03 $k_BT\,nm^{-2}$) [48], MD simulations (0.1–0.2 $k_BT\,nm^{-2}$) [23] and scaling arguments (0.1–1 $k_BT\,nm^{-2}$) [49]. Considering the two extreme estimations, a chlf surface concentration of 0.014–1.4 molecules nm^{-2} is required to result in a similar free energy contribution. Note that our simulations containing 0.26, 0.51 and 0.77 chlf per lipid corresponded to 1, 2 and 3 chlf molecules per nm^2 of membrane, respectively, so the suggested entropic effect is clearly captured.

4. Discussion

We have reported the results from CG–MD simulations of phase-segregating compositionally symmetric lipid membranes subjected to the effect of chlf. Chlf dramatically increases interleaflet interaction and results in pronounced phase symmetry between the membrane leaflets. We conjecture that this effect is due to an entropic mechanism that tries to avoid chlf confinement to one of the two leaflets. Chlf molecules rapidly jump from the lipid/water interfacial section of one leaflet to the lipid/water interface of the other. Such dynamic behaviour is highly favoured by the transversal colocalization of disordered domains where chlf molecules are preferentially placed.

The reported interleaflet coupling effect and its consequences in transmembrane lipid distribution, chol flip–flop rate, membrane curvature and internal mechanical properties could be of interest for the understanding of the consequences of adding chlf in many cellular functions, and in particular to understand its anaesthetic effect. The molecular mechanism of general anaesthesia is still an unresolved issue. Some proposals suggest that the anaesthetic compound changes the phasic state of the cell membrane, altering the activity of the lipid [50] and/or protein [51] ion channels involved in nerve transmission. Another aspect to take into account is that membrane proteins are distributed in a heterogeneous manner in the cell membrane and that alterations of this distribution may modify their functionality. In particular, there is experimental evidence that many ion channels involved in anaesthetic action are sorted and localized in specific lipid regions of the membrane [52]. In this context, Regen *et al*. showed that chlf laterally reorganizes

the lipid membrane matrix and suggested that such lipid rearrangement may be responsible for protein dysfunction leading to the anaesthetic effect [20]. Recent experiments in giant plasma membrane vesicles performed by Veatch *et al*. also point in a similar direction: some general anaesthetics alter the miscibility behaviour of a lipid membrane mixture, thus modifying its lipid arrangement at the nanometric scale [33].

The findings presented here contribute to the latter discussion by introducing a new aspect: the action of general anaesthetics could not only be related to the alteration of the lateral (in surface) lipid–protein organization, but also to changes in the transversal organization and structure of the bilayer. It is interesting to note that the comparison between chlf and its non-anaesthetic counterpart, ctcl, reveals that the interleaflet synchronizing effect is exclusively attributed to the anaesthetic compound. Actually, the main difference between many anaesthetics and their non-anaesthetic counterparts is that the former possess a dipole moment [53] that, according to the simulations, is responsible for the reported effect.

We are aware that our results are based on simulations containing chlf doses that are larger than those used in clinical applications. Physiological assays determined that an aqueous concentration of 5 mM of chlf is enough to block nerve conduction [54,55]. The partition coefficient of chlf between water and a lipid membrane was measured for DPPC bilayers giving a value of 30 [56], which would correspond to a chlf concentration of 150 mM inside the membrane phase. According to the volume of our simulated membranes, a ratio of about 0.09 chlf molecules per lipid is required to induce anaesthesia. In our simulations larger chlf doses of 0.77 chlf per lipid were used, and decreasing the amount of chlf also diminishes the interleaflet coupling effect. However, at the lowest simulated ratio (0.26 chlf per lipid, three times the nerve-blocking concentration), the effect is still rather significant (see the inset of figure 2): the variation of Λ from -0.35 (no chlf) to -0.20 (0.26 chlf per lipid) accounts for a significant increment of 23% in transversal phasic coincident area between leaflets.

In view of the large variety of proposed hypotheses to explain general anaesthesia, one could conjecture that the origin of the action of general anaesthesia is complex and manifold. Despite the limitations of our approach, the results presented here provide a novel and clear chlf-induced interleaflet synchronization effect that should be added to the list of plausible effects that may be involved in general anaesthesia. Further research on membrane systems with differing degrees of complexity (from simple protein-free lipid bilayers to *in vivo* cell membranes) must still be performed to examine these proposals in detail so that they can be validated or dismissed.

Acknowledgements. Computational resources were provided by the Barcelona Supercomputing Center (BSC).

Funding statement. Financial support is provided by SEID through project BFU2010-21847-C02-02 and by DURSI through project 2009-SGR-1055.

References

1. Harding AS, Hancock JF. 2008 Using plasma membrane nanoclusters to build better signaling circuits. *Trends Cell Biol.* **18**, 364–371. (doi:10.1016/j.tcb.2008.05.006)
2. Simons K, Ikonen E. 1997 Functional rafts in cell membranes. *Nature* **387**, 569–572. (doi:10.1038/42408)
3. Simons K, Toomre D. 2000 Lipid rafts and signal transduction. *Nat. Rev. Mol. Cell Biol.* **1**, 31–39. (doi:10.1038/35036052)
4. Anderson RG, Jacobson K. 2002 A role for lipid shells in targeting proteins to caveolae, rafts, and other lipid domains. *Science* **296**, 1821–1825. (doi:10.1126/science.1068886)
5. Munro S. 2003 Lipid rafts: elusive or illusive? *Cell* **115**, 377–388. (doi:10.1016/S0092-8674(03)00882-1)
6. May S. 2009 Transmonolayer coupling of fluid domains in lipid bilayers. *Soft Matter* **5**, 3148–3156. (doi:10.1039/b901647c)
7. Collins MD, Keller SL. 2008 Tuning lipid mixtures to induce or suppress domain formation across leaflets of unsupported asymmetric bilayers. *Proc. Natl Acad. Sci. USA* **105**, 124–128. (doi:10.1073/pnas.0702970105)
8. Perlmutter JD, Sachs JN. 2011 Interleaflet interaction and asymmetry in phase separated lipid bilayers: molecular dynamics simulations. *J. Am. Chem. Soc.* **133**, 6563–6577. (doi:10.1021/ja106626r)
9. Chiantia S, London E. 2012 Acyl chain length and saturation modulate interleaflet coupling in asymmetric bilayers: effects on dynamics and structural order. *Biophys. J.* **103**, 2311–2319. (doi:10.1016/j.bpj.2012.10.033)
10. Suzuki KGN, Fujiwara TK, Edidin M, Kusumi A. 2007 Dynamic recruitment of phospholipase Cγ at transiently immobilized GPI-anchored receptor clusters induces IP_3–Ca^{2+} signaling: single-molecule tracking study. *J. Cell Biol.* **177**, 731–742. (doi:10.1083/jcb.200609175)
11. Janmey PA, Kinnunen PKJ. 2006 Biophysical properties of lipids and dynamic membranes. *Trends Cell Biol.* **16**, 538–546. (doi:10.1016/j.tcb.2006.08.009)
12. Keller SL, Gruner SM, Gawrisch K. 1996 Small concentrations of alamethicin induce a cubic phase in bulk phosphatidylethanolamine mixtures. *Biochim. et Biophys. Acta* **1278**, 241–246. (doi:10.1016/0005-2736(95)00229-4)
13. Burack WR, Biltonen RL. 1994 Lipid bilayer heterogeneities and modulation of phospholipase A_2 activity. *Chem. Phys. Lipids* **73**, 209–222. (doi:10.1016/0009-3084(94)90182-1)
14. Brown MF. 1994 Modulation of rhodopsin function by properties of the membrane bilayer. *Chem. Phys. Lipids* **73**, 159–180. (doi:10.1016/0009-3084(94)90180-5)
15. Cantor RS. 1997 The lateral pressure profile in membranes: a physical mechanism of general anesthesia. *Biochemistry* **36**, 2339–2344. (doi:10.1021/bi9627323)
16. Iwamoto M, Oiki S. 2013 Amphipathic antenna on an inward rectifier K^+ channel responds to changes in the inner membrane leaflet. *Proc. Natl Acad. Sci. USA* **110**, 749–754. (doi:10.1073/pnas.1217323110)
17. Gruner SM, Shyamsunder E. 1991 Is the mechanism of general anesthesia related to lipid membrane spontaneous curvature? *Ann. N.Y. Acad. Sci.* **625**, 685–697. (doi:10.1111/j.1749-6632.1991.tb33902.x)
18. Reigada R. 2011 Influence of chloroform in liquid-ordered and liquid-disordered phases in lipid membranes. *J. Phys. Chem. B* **115**, 2527–2535. (doi:10.1021/jp110699h)
19. Reigada R. 2013 Atomistic study of lipid membranes containing chloroform: looking for a lipid-mediated mechanism of anesthesia. *PLoS ONE* **81**, e52631. (doi:10.1371/journal.pone.0052631)
20. Turkyilmaz S, Chen WH, Mitomo H, Regen SL. 2009 Loosening and reorganization of fluid phospholipid bilayers by chloroform. *J. Am. Chem. Soc.* **131**, 5068–5069. (doi:10.1021/ja9011468)
21. Lindahl E, Hess B, van der Spoel D. 2001 GROMACS 3.0: a package for molecular simulation and trajectory analysis. *J. Mol. Model.* **7**, 306–317.
22. Marrink SJ, Risselada HJ, Yefimov S, Tieleman DP, de Vries AH. 2007 The MARTINI force field: coarse grained model for biomolecular simulations. *J. Phys. Chem. B* **111**, 7812–7824. (doi:10.1021/jp071097f)
23. Risselada H, Marrink SJ. 2008 The molecular face of lipid rafts in model membranes. *Proc. Natl Acad. Sci.*

USA **105**, 17 367–17 372. (doi:10.1073/pnas.0807527105)

24. Marrink SJ, Tieleman DP. 2013 Perspective on the Martini model. *Chem. Soc. Rev.* **42**, 6801–6822. (doi:10.1039/c3cs60093a)
25. Yesylevskyy SO, Schäfer LV, Sengupta D, Marrink SJ. 2010 Polarizable water model for coarse-grained MARTINI force field. *PLoS Comput. Biol.* **6**, e1000810. (doi:10.1371/journal.pcbi.1000810)
26. Torrie GM, Valleau JP. 1977 Nonphysical sampling distributions in Monte Carlo free-energy estimation: umbrella sampling. *J. Comput. Phys.* **23**, 187–199. (doi:10.1016/0021-9991(77)90121-8)
27. Hub JS, de Groot BL, van der Spoel D. 2010 g_wham—a free weighted histogram analysis implementation including robust error and autocorrelation estimates. *J. Chem. Theory Comput.* **6**, 3713–3720. (doi:10.1021/ct100494z)
28. Vorobyov I, Bennett WFD, Tieleman DP, Allen TW, Noskov S. 2012 The role of atomic polarization in the thermodynamics of chloroform partitioning to lipid bilayers. *J. Chem. Theory Comput.* **8**, 618–628. (doi:10.1021/ct200417p)
29. Campelo F, Arnarez C, Marrink SJ, Kozlov MM. 2014 Helfrich model of membrane bending: from Gibbs theory of liquid interfaces to membranes as thick anisotropic elastic layers. *Adv. Colloid Interface Sci.* **208**, 25–33. (doi:10.1016/j.cis.2014.01.018)
30. Barnoud J, Rossi G, Marrink SJ, Monticelli L. 2014 Hydrophobic compounds reshape membrane domains. *PLoS Comput. Biol.* **10**, e1003873. (doi:10.1371/journal.pcbi.1003873)
31. Braun AR, Lacy MM, Ducas VC, Rhoades E, Sachs JN. 2014 α-Synuclein-induced membrane remodeling is driven by binding affinity, partition depth and interleaflet order asymmetry. *J. Am. Chem. Soc.* **136**, 9962–9972. (doi:10.1021/ja5016958)
32. Santo KP, Berkowitz ML. 2014 Shock wave interaction with a phospholipid membrane: coarse-grained computer simulations. *J. Chem. Phys.* **140**, 054906. (doi:10.1063/1.4862987)
33. Gray E, Karslake J, Machta BB, Veatch SL. 2013 Liquid general anesthetics lower critical temperatures in plasma membrane vesicles. *Biophys. J.* **105**, 2751–2759. (doi:10.1016/j.bpj.2013.11.005)
34. Lindblom G, Orädd G. 1994 NMR studies of translational diffusion in lyotropic liquid crystals and lipid membranes. *Prog. Nucl. Magn. Res. Spectr.* **26**, 483–515. (doi:10.1016/0079-6565(94)80014-6)
35. Lindblom G, Orädd G. 2009 Lipid lateral diffusion and membrane heterogeneity. *Biophys. Biochim. Acta* **1788**, 234–244. (doi:10.1016/j.bbamem.2008.08.016)
36. Kahya N, Scherfeid D, Bacia K, Poolman B, Schwille P. 2003 Probing lipid mobility of raft-exhibiting model membranes by fluorescence correlation spectroscopy. *J. Biol. Chem.* **278**, 28 109–28 115. (doi:10.1074/jbc.M302969200)
37. Almeida PF, Vaz WL, Thompson TE. 1992 Lateral diffusion in the liquid phase of DMPC/cholesterol lipid bilayers: a free volume analysis. *Biochemistry* **31**, 6739–6747. (doi:10.1021/bi00144a013)
38. Wohlert J, Edholm O. 2006 Dynamics in atomistic simulations of phospholipid membranes: nuclear magnetic resonance relaxation rates and lateral diffusion. *J. Chem. Phys.* **125**, 204703. (doi:10.1063/1.2393240)
39. Wang CY, Hill RJ. 2014 Transmembrane protein diffusion in gel-supported dual-leaflet membranes. *Biophys. J.* **107**, 2296–2304. (doi:10.1016/j.bpj.2014.10.016)
40. Wimley WC, Thompson TE. 1990 Exchange and flip-flop of dimyristoyl phosphatidylcholine in liquid-crystalline, gel and two-component, two-phase large unilamellar vesicles. *Biochemistry* **29**, 1296–1303. (doi:10.1021/bi00457a027)
41. Steck TL, Ye J, Lange Y. 2002 Probing red cell membrane cholesterol movement with cyclodextrin. *Biophys. J.* **83**, 2118–2125. (doi:10.1016/S0006-3495(02)73972-6)
42. Bennett WFD, MacCallum JL, Hinner MJ, Marrink SJ, Tieleman DP. 2009 Molecular view of cholesterol flip–flop and chemical potential in different membrane environments. *J. Am. Chem. Soc.* **131**, 12 714–12 720. (doi:10.1021/ja903529f)
43. Bennett WFD, Tieleman DP. 2012 Cholesterol translocation in a phospholipid membrane. *J. Lipid Res.* **53**, 421–429. (doi:10.1194/jlr.M022491)
44. Lange Y, Dolde J, Steck TL. 1981 The effect of cholesterol and other intercalated amphipaths on the contour and stability of the isolated red cell membrane. *J. Biol. Chem.* **256**, 5321–5323.
45. Khelashvili G, Kollmitzer B, Heftberger P, Pabst G, Harries D. 2013 Calculating the bending modulus for multicomponent lipid membranes in different thermodynamic phases. *J. Chem. Theory Comput.* **9**, 3866–3871. (doi:10.1021/ct400492e)
46. Fischer TM. 1992 Bending stiffness of lipid bilayers. I. Bilayer couple or single-layer bending? *Biophys. J.* **63**, 1328–1335. (doi:10.1016/S0006-3495(92)81710-1)
47. Patra M, Salonen E, Terama E, Vattulainen I, Faller R, Lee BW, Holopainen J, Karttunen M. 2006 Under the influence of alcohol: the effect of ethanol and methanol on lipid bilayers. *Biophys. J.* **90**, 1121–1135. (doi:10.1529/biophysj.105.062364)
48. Garbès Putzel G, Uline MJ, Szleifer I, Schick M. 2011 Interleaflet coupling and domain registry in phase-separated lipid bilayers. *Biophys. J.* **100**, 996–1004. (doi:10.1016/j.bpj.2011.01.021)
49. Collins MD. 2008 Interleaflet coupling mechanisms in bilayers of lipids and cholesterol. *Biophys. J.* **940**, L32–L34. (doi:10.1529/biophysj.107.124362)
50. Heimburg T. 2010 Lipid ion channels. *Biophys. Chem.* **150**, 2–22. (doi:10.1016/j.bpc.2010.02.018)
51. Seeger HM, Aldrovandi L, Alessandrini A, Facci P. 2010 Changes in single K^+ channel behavior induced by a lipid phase transition. *Biophys. J.* **99**, 3675–3683. (doi:10.1016/j.bpj.2010.10.042)
52. Li X, Serwanski DR, De Blas AL. 2007 Two pools of Triton X-100-insoluble GABAA receptors are present on the brain, one associated to lipid rafts and another one to the postsynaptic GABAergic complex. *J. Neurochem.* **102**, 1329–1345. (doi:10.1111/j.1471-4159.2007.04635.x)
53. North C, Cafiso DS. 1997 Contrasting membrane localization and behavior of halogenated cyclobutanes that follow or violate the Meyer–Overton hypothesis of general anesthetic potency. *Biophys. J.* **72**, 1754–1761. (doi:10.1016/S0006-3495(97)78821-0)
54. Seeman P. 1972 The membrane action of anesthetics and tranquilizers. *Pharmacol. Rev.* **24**, 583–655.
55. Reyes J, Latorre R. 1979 Effect of the anesthetics benzyl alcohol and chloroform on bilayers made from monolayers. *Biophys. J.* **28**, 259–280. (doi:10.1016/S0006-3495(79)85175-9)
56. Kamaya H, Kaneshina S, Ueda I. 1981 Partition equilibrium of inhalation anesthetics and alcohols between water and membranes of phospholipids with varying acyl chain-lengths. *Biochim. Biophys. Acta* **646**, 135–142. (doi:10.1016/0005-2736(81)90280-7)